to appear in AJ

An *HST* Census of Nuclear Star Clusters in Late-Type Spiral Galaxies: I. Observations and Image Analysis[1]

Torsten Böker[2], Seppo Laine, Roeland P. van der Marel

Space Telescope Science Institute, 3700 San Martin Drive, Baltimore, MD 21218, U.S.A.

boeker@stsci.edu, laine@stsci.edu marel@stsci.edu

Marc Sarzi, Hans-Walter Rix

Max-Planck-Institut für Astronomie, Königsstuhl 17, D-69117 Heidelberg, Germany

sarzi@mpia-hd.mpg.de, rix@mpia-hd.mpg.de

Luis C. Ho

Observatories of the Carnegie Institution of Washington, 813 Santa Barbara Street, Pasadena, CA 91101-1292, U.S.A.

lho@ociw.edu

Joseph C. Shields

Ohio University, Department of Physics and Astronomy, Clippinger Research Laboratories, 251B, Athens, OH 45701-2979

shields@helios.phy.ohiou.edu

ABSTRACT

We present new *HST* I-band images of a sample of 77 nearby, late-type spiral galaxies with low inclination. The main purpose of this catalog is to study the frequency and properties of nuclear star clusters. In 59 galaxies of our sample, we

[1]Based on observations made with the NASA/ESA *Hubble Space Telescope*, obtained at the Space Telescope Science Institute, which is operated by the Association of Universities for Research in Astronomy, Inc., under NASA contract NAS 5-26555. These observations are associated with proposal # 8599.

[2]Affiliated with the Astrophysics Division, Space Science Department, European Space Agency

have identified a distinct, compact (but resolved), and dominant source at or very close to their photocenter. In many cases, these clusters are the only prominent source within a few kpc from the galaxy nucleus. We present surface brightness profiles, derived from elliptical isophote fits, of all galaxies for which the fit was successful. We use the fitted isophotes at radii larger than $2''$ to check whether the location of the cluster coincides with the photocenter of the galaxy, and confirm that in nearly all cases, we are truly dealing with "nuclear" star clusters. From analytical fits to the surface brightness profiles, we derive the cluster luminosities after subtraction of the light contribution from the underlying galaxy disk and/or bulge.

Subject headings: galaxies: spiral — galaxies: structure — galaxies: nuclei — galaxies: star clusters — galaxies: statistics

1. Introduction

Over the past decade, high dynamic range observations with modern CCD detectors have shown that compact stellar nuclei are a common feature of spiral galaxies of all Hubble types. For example, Matthews & Gallagher (1997) found 10 objects with compact nuclear star clusters in a survey of 49 southern, very late-type spirals. However, as one progresses along the Hubble sequence towards earlier types, the increasingly luminous bulge component with its steeply rising surface brightness profile makes the identification of an additional, unresolved cluster extremely difficult. It therefore took the unique spatial resolution of the *Hubble Space Telescope (HST)* to demonstrate that nuclear clusters are a common phenomenon also in earlier Hubble types (e.g. Carollo, Stiavelli, & Mack 1998). The *HST* currently provides the only means to investigate the structural properties of nuclear star clusters, as demonstrated by Matthews et al. (1999), and to cleanly separate their emission from the underlying galaxy disk/bulge.

Despite the recent progress, the formation mechanism of nuclear star clusters remains largely a mystery. Intuitively, there are good reasons to expect matter accumulation in the deep gravitational wells of galaxies with massive bulges, and hence active star formation in their nuclei. In contrast, the gravitational force all but vanishes in the centers of pure disk galaxies with shallow surface brightness profiles and without any discernible bulge component. In these galaxies, the dynamical center is not a "special" place and it is far from obvious how a massive stellar cluster could have formed there. The shallow gravitational potential might provide a natural explanation for the fact that spirals of late Hubble type are not known to contain super-massive black holes. On the other hand, nuclear star clus-

ters can be extremely compact: the nucleus of M33, for example, has likely undergone core collapse and is as compact as any known globular cluster (Kormendy & McClure 1993). So far, no satisfying explanation has been put forward to explain the high gas densities that must have been present in the nuclei of these shallow disk galaxies to enable the formation of such massive and compact objects.

It is also unknown whether nuclear star clusters form repeatedly or only once - a question with important implications for the dynamical and morphological evolution of their host galaxies. To make progress along this line, it is essential to obtain the age distribution of nuclear star clusters. So far, reliable age estimates exist for only a handful of nuclear star clusters. Interestingly, most of them appear to be rather young: our Galaxy has a central stellar cluster with an age of only ~ 3 Myrs (Krabbe et al. 1995), and both M31 and M33 have blue nuclei that are very likely young star clusters (Lauer et al. 1998). More recently, we have published nuclear cluster ages derived from ground-based spectroscopy for IC 342 (≤ 60 Myrs, Böker, van der Marel, & Vacca 1999), and NGC 4449 ($6-10$ Myrs, Böker et al. 2001; Gelatt, Hunter, & Gallagher 2001). In addition, the dominant stellar population of the nuclear cluster in NGC 3227 is less than 50 Myrs old (Schinnerer, Eckard, & Tacconi 2001).

However, it is possible (and in fact quite likely) that ground-based observations predominantly target the brightest and hence youngest clusters. In order to get a more representative picture of nuclear star clusters, it is important to study a galaxy sample which is free from selection effects that favor the high end of the nuclear cluster luminosity range. In this paper, we describe the results of an *HST* I-band imaging survey of an unbiased sample of nearby, face-on, very late-type spirals (Scd or later). The main goals of the survey are (a) to determine the frequency of nuclear star clusters in very late-type spirals, (b) to derive their luminosity and size distribution, (c) to compare their properties to those of nuclear star clusters in earlier Hubble types which have been more extensively studied with *HST* (Carollo et al. 1997, 1998, 2001; Carollo 1999), and (d) to provide a source catalog for follow-up spectroscopic observations to age-date their stellar populations. The main purpose of this paper is to present the complete dataset. In a companion paper (Böker et al. 2002, in preparation), we describe the statistics of the full sample and investigate whether the properties of nuclear star clusters correlate in any way with those of their host galaxies.

This paper is organized as follows: in § 2, we describe our sample selection criteria, the observational strategy, and the data reduction procedure, and we present the final images as well as the results of the isophotal analysis. In § 3, we discuss whether the clusters indeed occupy the nuclei of their host galaxies, and how they compare to other luminous star clusters observed in a variety of starburst environments. We conclude in § 4.

2. Sample Selection, Observations and Data Reduction

2.1. The Sample

The target list for our survey was selected from the RC3 catalog of bright galaxies (de Vaucouleurs et al. 1991) according to the following criteria:

1. Hubble type between Scd and Sm ($6 \leq \mathrm{T} \leq 9$).
2. Line-of-sight velocity $\mathrm{v_{hel}} < 2000\,\mathrm{km\,s^{-1}}$, to assure good spatial resolution in physical units.
3. Axis ratio parameter $\mathrm{R_{25}} \equiv log(a/b) < 0.2$, i.e. inclination close to face-on. This helps to minimize the effects of dust extinction due to the galaxy disk, and to avoid confusion in the identification of the nucleus from line-of-sight projection of disk clusters.

Our sample is unbiased with respect to galaxy size, mass, total magnitude, star formation efficiency, or any other quantity that might reasonably be expected to favor or disfavor nuclear cluster formation. It should therefore be well suited to provide an objective census of nuclear clusters in late-type galaxies in the local universe.

We identified a total of 113 galaxies which satisfied the above criteria and had not previously been observed with the Wide Field and Planetary Camera 2 (WFPC2) onboard *HST* in the F814W filter. These 113 galaxies were used as the target pool for our WFPC2 snapshot program (GO-8599). To date, 77 galaxies have been successfully observed, listed in Table 1. It is possible that a few more targets will be observed later, but for this paper, we limited the sample to those galaxies observed before August 3, 2001.

2.2. The WFPC2 Images

All images were taken with the WFPC2 camera onboard *HST*, with the galaxy nucleus centered on the Planetary Camera (PC) chip. The PC pixel size is $0.046''$, and the field of view is $36'' \times 36''$. We used the F814W filter with an integration time of 600 s, split in two exposures of 300 s to allow cosmic ray rejection. We also took a short exposure (40 s) to guard against saturation of the WFPC2 detectors in the 300 s exposures. However, none of the galaxies was bright enough to require the use of the 40 s exposure. The PSF with the F814W filter has a FWHM of $0\overset{''}{.}07$.

We used the STSDAS task `wfixup` to interpolate (in the x-direction) over bad pixels as identified in the data quality files. We also used the STSDAS task `warmpix` to correct

consistently warm pixels in the data, using the most recent warm pixel tables which are provided by the WFPC2 instrument group at STScI about once a month. The STSDAS task `ccrej` was used to combine the two 300 s exposures. This step corrects most of the pixels affected by cosmic rays in the combined image. In general, a few cosmic rays remain uncorrected, mostly when the same pixel was hit in both exposures. Also, a small number of hot pixels remain uncorrected because they are not listed even in the most recent warm pixel tables. We corrected these with the IRAF task `cosmicrays`, setting the "threshold" and "fluxratio" parameters to suitable values that were selected by careful comparison of the images before and after correction to ensure that only questionable pixels were replaced. The photometric calibration, and conversion to Johnson I-band was performed according to Holtzman et al. (1995). We assumed a standard color of $\mathrm{V}-\mathrm{I}=1$ for the galaxies which translates into a zeropoint of 21.55 (note that the assumed color affects the zeropoint only weakly: a color of $\mathrm{V}-\mathrm{I}=2$ would result in a zeropoint of 21.56).

After visual inspection of the images, we divided the objects into two groups. The first group contains those 59 objects for which a) the (photo-) center of the galaxy is reasonably well defined, and b) a prominent, isolated point-like source can be identified close to it. These sources are nuclear cluster candidates. In § 3.1, we will discuss our criteria for whether they are indeed occupying the photocenter or not.

The second group contains the remaining 18 galaxies which show no easily identifiable source close to the center. This does not necessarily mean that these galaxies do not harbor a nuclear cluster; it merely indicates that we cannot identify one with any kind of certainty from our data. Figures 1 and 2 contain the images of the 59 (18) galaxies in group 1 (2).

Visual inspection of the images reveals a number of noteworthy points:

1. In most cases, the nuclear star cluster candidate is obvious in the images, because it is the dominant source at or close to the photocenter of the galaxy. It is often (but not always) the brightest source in the field, and in many cases the only cluster within a kpc from the photocenter.

2. For the vast majority of the sample galaxies, the images show no morphological evidence for a stellar bulge. While our sample was obviously selected to avoid bright stellar bulges, it is still surprising that there appears to be no bulge at all in many late-type spirals. The visual impression is confirmed by the surface brightness analysis in § 2.3. Our dataset is uniquely suited for a detailed investigation of the structural properties of late-type spiral galaxies which is, however, beyond the scope of this paper. We defer a more detailed study of the disk surface brightness, the (lack of) evidence for stellar bulges, and possible correlations with nuclear cluster properties to a later

paper (Stanek et al. 2002, in preparation).

3. In many cases (e.g. UGC 3574, UGC 5015, or NGC 4411B), the nuclear cluster is "naked": it forms a distinct entity that appears completely isolated within the disk. The cluster location does not appear to be a dynamically "special" place, because there are no spiral arms, dust lanes, or other signs of a kinematic center visible in the images. This is even true at the smallest spatial scales as observed in the most nearby galaxies, such as NGC 300 or NGC 7793. This confirms a notion by Matthews et al. (1999) who studied a sample of four extreme late-type spirals, also with WFPC2.

4. In other cases (e.g. NGC 853, NGC 2139, or NGC 4027), however, the cluster location seems to be the origin of spiral structure or prominent dust lanes, indicative of it being at the dynamical center of the galaxy. If the mechanisms that lead to such a morphology are in any way connected to the presence of a nuclear cluster, it appears that they are a consequence rather than the prerequisite of nuclear cluster formation, because it is difficult to imagine how a galaxy like NGC 2139 can change its structure back to the smooth and regular appearance of those with "naked" nuclear clusters.

2.3. Isophotal Fits

We used the IRAF-task `ellipse` to obtain surface brightness profiles (SBP) over the PC field of view for all galaxies in our sample. For the galaxies in group 1, we started the fitting process centered on the cluster with a semi-major axis (SMA) length of 5 pixels ($0\farcs23$). We varied the SMA length logarithmically (with a 15% stepsize), first going out to a maximum SMA of 350 pixels ($\approx 16''$), then inwards to the sampling limit (SMA of 0.5 pixels or $0\farcs023$). Throughout the fit, the ellipse center, ellipticity, and position angle were allowed to vary freely. By comparing the position of the peak surface brightness (i.e. the position of the putative nuclear cluster) to the center of the outer isophotes, we were able to decide whether the cluster indeed occupies the photocenter of the galaxy. This is further discussed in § 3.1.

For a small number of galaxies, such an unconstrained fit failed for a small range of radii, typically because of a complex morphology, a shallow surface brightness gradient, a low signal-to-noise ratio, or any combination of these factors. In these cases, we performed two fits, one as described above, and going out as far as possible, and a second fit starting at a large radius, going inward as far as possible. By combining the two fits, we were able to construct the SBP over most of the radial range, with data missing for only a few radii. For another small group of galaxies, we were forced to increase the spacing between isophotes (stepsize of 50%) to overcome the low signal-to-noise ratio.

The 18 galaxies in group 2 have no plausible candidate for a nuclear cluster. These are mostly objects with very low surface brightness and an ill-defined photocenter. In these cases, we proceeded as follows: we first derived an estimate for the photocenter and ellipticity of the galaxy from the average of three isophotes at large radii (typically 200 pixels plus or minus 15%). The SBP was then derived from a second fit for which the isophote center and ellipticity was fixed to the initial estimates. This procedure worked for all but four galaxies, for which it was impossible to obtain even an estimate for the photocenter. One of these (ESO 510-59) appears to be a merger pair, one (NGC 6946) contains large amounts of dust in the nucleus, and the other two (A 1301-03, and IC 4182) are too faint in our images to detect a meaningful SB gradient.

In Figures 3 and 4, we show the resulting SBPs for all galaxies in group 1 and 2, respectively. The presence of the nuclear cluster candidate is obvious by the sharp upturn in the SBPs of Figure 3, typically at radii around $0\farcs3$. Not surprisingly, the clear upturn is absent in the profiles of the group 2 galaxies in Figure 4. Their SBPs are in general noisier, and in some cases even decrease in brightness towards the center, just another manifestation of their shallow surface brightness gradients.

2.4. Photometry of the Nuclear Clusters

For the derivation of the luminosity of the nuclear clusters it is useful to have a parametrized fit to the SBP. For this, we used the form

$$I(r) = I_0 \cdot (r/r_b)^{-\gamma} \cdot (1 + (r/r_b)^{\alpha})^{\frac{\gamma-\beta}{\alpha}} \cdot (1 + (r/r_c)^{\delta})^{\frac{\beta-\epsilon}{\delta}}. \tag{1}$$

This is based on the so-called 'nuker-law' parametrization (Lauer et al. 1995; Byun et al. 1996), which represents a broken power-law with an inflection point at a radius r_b. We added an additional factor which allows for the possibility of a second inflection point at a radius r_c. The resulting equation was found to be sufficiently general for the purposes of this paper.

In general, the presence of a nuclear cluster causes a distinct upturn in the SBP at a certain radius $R_{\rm u}$. This radius was identified by eye for each galaxy, the adopted values are listed in Column 5 of Table 2. To estimate the cluster luminosity, we started by fitting the parametrization (1) to the data inside $R_{\rm u}$ (dotted curves in Figure 3), followed by integration over an aperture with radius $R_{\rm u}$. To obtain an estimate for the nuclear cluster luminosity, one needs to subtract from this the light contribution of the galaxy disk (and possibly bulge) within $R_{\rm u}$. To this end, we considered two models for the SBP of the underlying galaxy light within the PC field of view which are likely to bracket the true SBP of the galaxy. For the first model, we assumed that the underlying galaxy has a constant surface brightness inside

$R_{\rm u}$ (dashed lines in Figure 3). For the second model, we performed a fit of a nuker-law to the data outside $R_{\rm u}$, and extrapolated that fit to radii inside $R_{\rm u}$ (solid curves in Figure 3).

After subtraction of the integrated luminosity inside $R_{\rm u}$ of the two models for the underlying galaxy light, we obtain two different estimates for the nuclear cluster luminosity. In Table 2, we list the mean of these two estimates and also half their difference as a measure of the uncertainty. The latter uncertainty indicates only the extent to which the cluster photometry depends on the choice of underlying galaxy model. In general, this is not the dominant source of error. The uncertainty due to the exact choice of the aperture size $R_{\rm u}$ adds at least 0.1 mag of error to the nuclear cluster luminosity estimates.

In Figure 5, we plot histograms of both apparent and absolute cluster luminosity. The distribution has a FWHM of about 4 magnitudes, with a median of $\rm M_I = -11.5$. This is brighter than even the brightest globular cluster in the Milky Way, but comparable to the bright end of the cluster luminosity function in the NGC 4038/39 merging system (Whitmore et al. 1999) or the young super star clusters in M 82 (O'Connell et al. 1995). An absolute luminosity of $\rm M_I = -11.5$ corresponds to $1.6 \cdot 10^6\ \rm L_\odot$ in the I-band (because $\rm M_{\it I,\odot} = 4.02$). The associated mass depends on the unknown mass-to-light ratio M/L. For reference, one can consider the case of a cluster formed in an instantaneous burst with a Salpeter (1955) initial mass function and solar metallicity. For a young cluster with an age of 10 Myr one then has $M/L_I \approx 0.016$ and $M = 2.6 \cdot 10^4\ \rm M_\odot$, whereas for an old cluster with an age of 5 Gyr one has $M/L_I \approx 0.43$ and $M = 6.9 \cdot 10^5\ \rm M_\odot$ (Leitherer et al. 1999). Our ongoing spectroscopic program to derive cluster ages for many of the sample galaxies promises to remove this ambiguity.

Photometry of the off-nuclear clusters in the low surface brightness disks of the group 2 galaxies, e.g. in UGC 12082 or ESO 187-51, shows that we can easily detect clusters as faint as $\rm M_I = -8$. However, none of the galaxies in group 2 shows any evidence for *nuclear* clusters in this luminosity range. This demonstrates that the low-luminosity cutoff in Figure 5b around $\rm M_I = -9$ is probably real.

2.5. The size of nuclear star clusters

To derive physically meaningful information about the structural properties of nuclear clusters such as the half-light radius or the core radius in a King model, the observed SBPs have to be corrected for the instrumental point spread function (PSF). Since the clusters in most cases are not much more extended than the *HST* PSF, and the shape of the PSF is rather complex because of its extended wings, the deconvolution is a non-trivial task which

we defer to a later paper (Sarzi et al. 2002, in preparation).

For now, we list in Table 2 a simple measure of the nuclear cluster sizes, namely the half-width-at-half-maximum (HWHM), i.e. the radius at which the *observed* surface brightness drops to half its peak value. These were derived using simple linear interpolation between the two datapoints in the SBP that bracket half the peak value of the surface brightness. The listed values can be compared to those for the *HST* PSF. We constructed a PSF model from the TinyTim software package (Krist & Hook 2001) for the PC chip and the F814W filter, and performed an identical isophotal fit. The resulting HWHM was $0\farcs032$. For comparison, an identical analysis for a bright star in the image of the galaxy NGC 6509 yields $0\farcs036$. Both values are smaller than those listed in Table 2, which confirms that the nuclear clusters are indeed resolved.

Figure 6a contains a histogram of the angular HWHM distribution which is strongly peaked around $0\farcs06$. We caution that the complexity of the *HST* PSF (which is only poorly represented by a single Gaussian) makes the simple approach of quadratically subtracting the HWHM of the PSF from the observed one to obtain a measure of the intrinsic cluster size unreliable. Nevertheless, it is already clear from this simple analysis that the clusters are very compact, with typical intrinsic HWHM values of around 5 pc (Figure 6b).

As a whole, the nuclear clusters appear to be a very homogeneous class, not only in luminosity, but also in their structural parameters. The absence of unresolved nuclear sources in late-type galaxies - as suggested by this preliminary analysis - suggests that any accretion-powered emission from active galactic nuclei (AGN) is optically weak in most galaxies of late Hubble types.

3. Discussion

3.1. Are the clusters truly nuclear?

The question of whether the clusters are indeed located at the photometric center of their respective host galaxy is not easily answered, because the term “photometric center” is not well defined itself. For our analysis, we have defined the photometric center as the average isophote center of our `ellipse` fit results for radii between $2''$ (well beyond the extent of the cluster) and that of the outermost fitted ellipse - in most cases around $15''$. For the median distance of our sample, this radial range corresponds to linear scales between 200 pc and 1.5 kpc. If present, a stellar bar is likely to dominate the luminosity within this range, but since in the absence of close interactions a bar should be symmetric with respect to the dynamical center, its photocenter is likely a good measure of the true galaxy nucleus.

Figure 7a shows a histogram of the projected angular distance between the position of the presumed nuclear cluster and the galaxy photocenter according to the definition above. About 75% (45 out of 59) clusters lies within $1''$ from the photocenter. This angular separation corresponds to about 90 pc at the median distance of our sample (19 Mpc). In this representation, some clusters appear to be well-separated from the galaxy center. However, we caution that in many galaxies of our sample, the photocenter is poorly defined, and its position very uncertain.

In order to visualize the uncertainties in the photocenter positions, we show in Figure 7b a plot of the projected offset between photocenter and nuclear cluster for all galaxies in group 1. Here, the size of the crosses indicates the standard deviation σ in the image x and y directions of the isophote centers measured from isophotes at radii $\geq 2''$. If one assumes that the isophote centers are subject to random measurement errors, then the error in the photocenter position should be $\sigma/\sqrt{n}$, where n is the number of isophotes. However, the isophotal fits are clearly influenced by dust lanes, extended star formation, or other asymmetries that vary with isophote radius, and thus make the determination of the photocenter of an individual galaxy subject to systematic uncertainties. We therefore have conservatively estimated the error in the photocenter position to equal σ, without dividing by $\sqrt{n}$.

The fact that this estimate is indeed a conservative one is demonstrated in Figure 7c which shows the cumulative distribution of cluster positions inside a certain number of standard deviations. The observed sample is compared to the expected curve for a two-dimensional normal (i.e. Gaussian) error distribution. The observed distribution is narrower than the prediction which indicates that we have somewhat overestimated our errors in determining the photocenter.

While this analysis does not prove that each individual cluster does indeed occupy the true nucleus of its host galaxy, the results demonstrate that the majority of clusters are - within the errors - located at or very near the photometric center. In the absence of any kinematical information, it is reasonable to assume that the photocenter coincides with the dynamical center. We therefore conclude that these clusters can rightfully be called "nuclear".

3.2. Are nuclear clusters special?

One of the most interesting results from *HST* imaging has been the discovery of extremely luminous, compact, young star clusters in a variety of starburst environments, in-

cluding merging galaxies (Conti & Vacca 1994; Whitmore et al. 1999), dwarf galaxies (Hunter et al. 1994; Calzetti et al. 1997), and in the circumnuclear rings of nearby spiral galaxies (Barth et al. 1995; Buta et al. 2000; Maoz et al. 2001). Prior to *HST*, only a few objects of this type were known to exist (Arp & Sandage 1985; Melnick et al. 1985); the severe crowding in most starbursts made it impossible to resolve the individual clusters in ground-based images. Such "super star clusters" apparently form preferentially during extreme episodes of violent star formation and may be the basic building blocks of starbursts. Barely resolved by *HST*, they have effective radii of only $2 - 4$ pc and luminosities that range as high as $M_V = -14$ to -15 mag. The small radii, high luminosities, and presumably high masses of these clusters have led to suggestions that they may remain as bound systems and therefore could be present-day versions of young globular clusters (e.g. Ho & Filippenko 1996).

The nuclear clusters discovered in our survey bear a close resemblance to off-nuclear super star clusters. Although we do not yet have definitive size measurements for our sources, the observed HWHM values range from $\sim$1 to 10 pc, with a median value of $\sim$5 pc; this is consistent with the sizes of super star clusters. Similarly, the optical absolute magnitudes of the nuclear clusters lie comfortably within the luminosity function of super star clusters.

4. Conclusions

We have presented a catalog of *HST*/WFPC2 I-band images of an unbiased sample of 77 nearby, late-type spiral galaxies with low inclination. From an isophotal analysis of the images, we demonstrate that about 75% of the sample galaxies host a compact, luminous stellar cluster at or very close to their photocenter. These clusters often are completely isolated from other comparable structures, emphasizing that even in the relatively shallow potential wells of late-type galaxy disks, the center is well-defined, and has a unique star formation history. From analytical fits to the surface brightness profiles, we determine the flux attributable to the cluster. The distribution of absolute cluster luminosities has a FWHM of 4 magnitudes, and a median value of $\mathrm{M_I} = -11.5$, comparable to young super star clusters in starbursting galaxies. Together with initial estimates of their size distribution, this suggests that nuclear clusters in spiral galaxies of the latest Hubble types are a fairly homogenous class of objects. The dataset is a representative survey of late-type spiral galaxies in the local universe, and as such yields a valuable source catalog for spectroscopic follow-up observations which are needed to further constrain the star formation history of nuclear clusters. We have begun such a follow-up program both with *HST* and ground-based observatories.

The anonymous referee provided useful comments which helped to improve the presentation of this paper. Support for proposal # 8599 was provided by NASA through a grant from the Space Telescope Science Institute, which is operated by the Association for Research in Astronomy, Inc., under NASA contract no. NAS 5-26555. This research has made use of the NASA/IPAC Extragalactic Database (NED) which is operated by the Jet Propulsion Laboratory, California Institute of Technology, under contract with NASA. It has also benefited greatly from use of the Lyon-Meudon Extragalactic Database (LEDA, http://leda.univ-lyon1.fr).

REFERENCES

Armandroff, T. E. 1989, AJ, 97, 357

Arp, H. & Sandage, A. 1985, AJ, 90, 1163

Barth, A. J., Ho, L. C., Filippenko, A. V., & Sargent, W. L. W. 1995, AJ, 110, 1009

Böker, T., van der Marel, R. P., & Vacca, W. D. 1999, AJ, 118, 831

Böker, T., van der Marel, R. P., Mazzuca, L., Rix, H.-W., Rudnick, G., Ho, L., & Shields, J. C. 2001, AJ, 121, 1473

Buta, R., Treuthardt, P. M., Byrd, G. G., & Crocker, D. A. 2000, AJ, 120, 1289

Byun, Y.-I., et al. 1996, AJ, 111, 1889

Calzetti, D., Meurer, G., Bohlin, R. C., Garnett, D., Kinney, A. L., Leitherer, C., & Storchi-Bergmann, T. 1997, AJ, 114, 1834

Cardelli, J. A., Clayton, G. C., & Mathis, J. S. 1989, ApJ, 345, 245

Carignan, C. 1985, ApJS, 58, 107

Carollo, C. M. 1999, ApJ, 523, 566

Carollo, C. M., Stiavelli, M., de Zeeuw, P. T., & Mack, J. 1997, AJ, 114, 2366

Carollo, C. M., Stiavelli, M., & Mack, J. 1998, AJ, 116, 68

Carollo, C. M., Stiavelli, M., de Zeeuw, P. T., Seigar, M., & Dejonghe, H. 2001, ApJ, 546, 216

Conti, P. S., & Vacca, W. D. 1994, ApJ, 423, L97

de Vaucouleurs, G. 1948, Ann. d'Astrophysique, 11, 247

de Vaucouleurs, G. 1963, ApJ, 137, 720

de Vaucouleurs, G., de Vaucouleurs, A., Corwin, H., Buta, R. J., Paturel, G., & Fouque, P. 1991, *Third Reference Catalogue of Bright Galaxies*, New York:Springer-Verlag

Freedman, W. L., Madore, B. F., Hawley, S. L., Horowitz, I. K., Mould, J., Navarrete, M., & Sallmen, S. 1992, ApJ, 396, 80

Gelatt, A. E., Hunter, D. A., & Gallagher, J. S. 2001, PASP, 113, 142

Ho, L. C., & Filippenko, A. V. 1996, ApJ, 472, 600

Holtzman, J. A., Burrows, J., Casertano S., Hester, J. J., Trauger J. T., Watson, A. M., Worthey, G. 1995, PASP, 107, 1065

Hunter, D. A., O'Connell, R. W., & Gallagher, III, J. S. 1994, AJ, 108, 84

Kormendy. J. & McClure, R. D. 1993, AJ, 105, 1793

Krabbe, A. et al. 1995, ApJ, 447, L95

Krist, J. & Hook, R. 2001, The TinyTim User's Guide, Version 6.0 (Baltimore:STScI)

Lauer, T. R., et al. 1995, AJ, 110, 2622

Lauer, T. R., Faber, S. M., Ajhar, E. A., Grillmair, C. J., & Scowen, P. A. 1998, AJ, 116, 2263

Leitherer, C., et al. 1999, ApJS, 123, 3

Maoz, D., Barth, A. J., Ho, L. C., Sternberg, A., & Filippenko, A. V. 2001, AJ, 121, 3048

Matthews, L. D. & Gallagher, J. S., III 1997, AJ, 114, 1899

Matthews, L. D. et al. 1999, AJ, 118, 208

Melnick, J., Moles, M., & Terlevich, R. 1985, A&A, 149, L24

O'Connell, R. W., Gallagher, J. S., Hunter, D. A., & Colley, W. A. 1995, ApJL, 446, L1

Phillips, A.C., Illingworth, G. D., MacKenty, J. W., & Franx, M. 1996, AJ, 111, 1566

Salpeter, E. E. 1955, ApJ, 121, 161

Sandage A., & Tammann G. 1990, ApJ, 365, 1

Schinnerer, E., Eckard, A., & Tacconi, L. J. 2001, ApJ, 549, 254

Schlegel, D. J., Finkbeiner, D. P., & Davis, M. 1998, ApJ, 500, 525

Tully, R. B. 1988, Nearby Galaxies Catalog (Cambridge: Cambridge Univ. Press)

Whitmore, B. C., Zhang, Q., Leitherer, C., Fall, S. M., Schweizer, F., & Miller, B. W. 1999, AJ, 118, 1551

Fig. 1.— WFPC2 F814W images of the 59 galaxies with evidence for a nuclear cluster. The bar in the upper left corner represents a scale of 1 kpc, calculated from the distances listed in Table 2. For a few very nearby objects, the bar is dashed, in which case it indicates a scale of 250 pc. The symbol in the top right corner indicates north (with arrow) and east directions. All images are on a logarithmic grey-scale stretch, optimized for the dynamic range of the galaxy. The object identified as the central cluster is circled in sources where a visual identification may be ambiguous.

Fig. 2.— As Figure 1 for the 18 galaxies without evidence for a nuclear cluster.

Fig. 3.— I-band surface brightness profiles (SBP) of the 59 galaxies with evidence for a nuclear cluster. The diamond-shaped symbols indicate the results of the elliptical isophote fits. The formal error bars of the isophote fits are also shown; in most cases, they are contained within the symbol size. The lines show the best fit analytical model to the inner part of the SBP as described in § 2 (dotted), the inward-extrapolated best fit outside of the nuclear cluster (solid), and the constant surface brightness level (dashed) at the radius where the SBP starts to deviate from the pure disk profile. This radius was used to derive the cluster luminosity as described in § 2.4.

Fig. 4.— As Figure 3 for those 14 galaxies in group 2 (without evidence for a nuclear cluster) for which the isophotal fit was successful.

Fig. 5.— Histogram of apparent (left) and absolute (right) I-band magnitudes of all identified nuclear clusters. Also shown are the median absolute luminosity of the sample (asterisk) and the luminosity of a cluster with 10^6 and 10^7 $L_\odot$, respectively (diamonds).

Fig. 6.— Histogram of angular (left) and linear (right) observed HWHM radius (i.e. not corrected for PSF convolution) of all identified nuclear clusters. The vertical dashed line in the left panel denotes the HWHM radius of the F814W PSF.

Fig. 7.— a) distribution of projected distances between nuclear cluster position and the average isophote center between $2''$ and $15''$. b) projected position of all nuclear clusters, relative to the photocenter of their respective host galaxy. The size of the crosses denotes the 1σ scatter in the isophote centers. c) cumulative distribution of projected distance between cluster and photocenter (solid curve), compared to the expected curve for a two-dimensional Gaussian error distribution (dotted curve).

Table 1. Summary of Observations

(1) Galaxy	(2) R.A. (J2000)	(3) Dec. (J2000)	(4) v_z [km/s]	(5) Type	(6) m_B [mag]	(7) A_I [mag]	(8) d_{MA} [arcmin]	(9) Obs. date
NGC 275	00 51 04.20	-07 04 00.0	1681	SB(rs)cd pec	13.16	0.109	1.5	07/09/01
NGC 300	00 54 53.47	-37 41 00.0	-54	SA(s)d	8.95	0.025	21.9	05/06/01
NGC 337a	01 01 33.90	-07 35 17.7	998	SAB(s)dm	14.92	0.189	5.9	07/10/01
NGC 428	01 12 55.60	-00 58 54.4	1130	SAB(s)m	11.91	0.055	4.1	01/06/01
NGC 450	01 15 30.52	-00 51 38.3	1720	SAB(s)cd:	12.20	0.077	3.1	07/12/01
ESO 80-6	01 47 16.87	-62 58 14.8	1227	SB(s)m	14.37	0.052	1.4	07/10/01
NGC 600	01 33 05.25	-07 18 42.1	1763	SB(rs)d	13.65	0.073	3.3	07/09/01
NGC 853	02 11 43.35	-09 18 01.1	1413	Sm pec	13.43	0.050	1.5	07/10/00
NGC 1042	02 40 23.63	-08 25 59.8	1271	SAB(rs)cd	12.50	0.056	4.7	01/26/01
NGC 1313	03 18 15.37	-66 29 50.6	174	SB(s)d	9.20	0.212	9.1	01/12/01
ESO 358-5	03 27 16.47	-33 29 06.1	1409	SAB(s)m pec:	14.90	0.022	1.4	05/31/01
ESO 418-8	03 31 30.48	-30 12 44.6	988	SB(r)d	13.68	0.029	1.2	05/30/01
NGC 1493	03 57 27.73	-46 12 38.1	796	SB(rs)cd	11.78	0.020	3.5	05/02/01
ESO 202-41	04 36 56.69	-52 10 25.2	1396	SB(s)m	14.94	0.017	1.2	04/27/01
ESO 85-47	05 07 43.86	-62 59 24.3	1180	SB(s)m	14.53	0.050	1.7	04/26/01
ESO 204-22	05 36 26.06	-52 11 02.5	1005	SB(s)m: pec	15.44	0.080	1.3	12/25/00
NGC 2139	06 01 07.90	-23 40 21.3	1649	SAB(rs)cd	11.99	0.065	2.6	02/15/01
UGC 3574	06 53 10.60	+57 10 39.0	1635	SA(s)cd	13.20	0.103	4.2	01/30/01
UGC 3826	07 24 32.05	+61 41 35.2	1946	SAB(s)d	14.10	0.133	3.5	10/06/00
NGC 2552	08 19 20.14	+50 00 25.2	695	SA(s)m?	12.56	0.090	3.5	04/06/01
UGC 4499	08 37 41.43	+51 39 11.1	877	SAdm	13.50	0.069	2.6	05/31/01
NGC 2763	09 06 49.26	-15 29 59.9	1769	SB(r)cd pec	12.64	0.141	2.3	04/02/01
NGC 2805	09 20 24.56	+64 05 55.2	1968	SAB(rs)d	11.52	0.100	6.3	10/07/00
UGC 4988	09 23 15.26	+34 44 03.7	1696	SABm	15.30	0.036	1.1	06/03/01
UGC 5015	09 25 47.89	+34 16 35.9	1800	SABdm	14.90	0.034	1.9	06/04/01
UGC 5288	09 51 17.00	+07 49 39.0	559	Sdm:	14.09	0.066	1.3	01/14/01
NGC 3206	10 21 47.65	+56 55 49.6	1380	SB(s)cd	12.57	0.027	3.0	05/14/01
NGC 3346	10 43 38.90	+14 52 18.0	1315	SB(rs)cd	12.41	0.054	2.9	01/14/01
NGC 3423	10 51 14.30	+05 50 24.0	1025	SA(s)cd	11.59	0.058	3.8	02/07/01
NGC 3445	10 54 35.87	+56 59 24.4	2245	SAB(s)m	12.90	0.015	1.6	06/01/01
NGC 3782	11 39 20.72	+46 30 48.6	944	SAB(s)cd:	13.10	0.035	1.7	05/10/01
NGC 3906	11 49 40.46	+48 25 33.3	1166	SB(s)d	13.49	0.050	1.9	03/09/01
NGC 3913	11 50 38.77	+55 21 12.1	1190	SA(rs)d:	13.17	0.025	2.6	01/17/01
A 1156+52	11 59 09.47	+52 42 26.1	1307	SB(rs)cd	13.12	0.053	3.5	08/03/01
ESO 504-30	11 57 15.14	-27 42 00.2	1673	SB(r)d:	14.66	0.142	1.1	05/06/01
UGC 6931	11 57 22.79	+57 55 22.5	1446	SBm:	14.31	0.049	1.4	08/16/00
NGC 4027	11 59 30.50	-19 15 44.0	1588	SB(s)dm	11.66	0.081	3.2	04/07/01
NGC 4204	12 15 14.51	+20 39 30.7	968	SB(s)dm	12.90	0.065	3.6	06/11/01
NGC 4299	12 21 40.90	+11 30 03.0	306	SAB(s)dm:	12.88	0.063	1.7	04/28/01
NGC 4416	12 26 46.72	+07 55 07.9	1449	SB(rs)cd:	13.14	0.049	1.7	03/19/01
NGC 4411B	12 26 47.30	+08 53 04.5	1334	SAB(s)cd	12.91	0.058	2.5	05/28/01
NGC 4487	12 31 04.36	-08 03 13.8	1020	SAB(rs)cd	12.26	0.041	4.2	05/28/01
NGC 4496A	12 31 39.32	+03 56 22.7	1772	SB(rs)m	11.94	0.048	4.0	03/17/01
NGC 4517A	12 32 28.15	+00 23 22.8	1554	SB(rs)dm:	12.94	0.046	4.0	03/18/01
NGC 4540	12 34 50.90	+15 33 06.9	1383	SAB(rs)cd	12.44	0.065	1.9	07/19/00
NGC 4618	12 41 32.74	+41 09 03.8	748	SB(rs)m	11.22	0.041	4.2	07/10/01
NGC 4625	12 41 52.61	+41 16 26.3	816	SAB(rs)m pec	12.92	0.035	2.2	05/28/01

Table 1—Continued

(1) Galaxy	(2) R.A. (J2000)	(3) Dec. (J2000)	(4) v_z [km/s]	(5) Type	(6) m_B [mag]	(7) A_I [mag]	(8) d_{MA} [arcmin]	(9) Obs. date
NGC 4701	12 49 11.71	+03 23 21.8	768	SA(s)cd	12.80	0.057	2.8	05/29/01
NGC 4775	12 53 45.79	-06 37 20.1	1565	SA(s)d	12.24	0.067	2.1	12/21/00
NGC 4904	13 00 56.97	-00 01 31.9	1204	SB(s)cd	12.60	0.050	2.2	07/12/00
A 1301-03	13 04 31.43	-03 34 20.3	1379	SAB(s)dm	12.90	0.058	3.5	06/02/01
IC 4182	13 05 49.53	+37 36 17.6	515	SA(s)m	13.0	0.027	6.0	07/09/01
ESO 444-2	13 16 44.91	-27 53 09.7	1544	SAB(s)dm	14.97	0.142	1.1	05/30/01
NGC 5068	13 18 54.60	-21 02 19.7	607	SB(s)d	10.52	0.197	7.2	06/02/01
UGC 8516	13 31 52.50	+20 00 01.0	1156	Scd:	14.03	0.057	1.1	06/01/01
ESO 510-59	14 04 46.43	-24 49 40.7	2267	SB(s)cd	13.61	0.138	2.5	04/27/01
NGC 5477	14 05 31.25	+54 27 12.3	565	SA(s)m	14.36	0.021	1.7	09/22/00
NGC 5585	14 19 48.08	+56 43 43.8	571	SAB(s)d	11.20	0.030	5.8	05/05/01
NGC 5584	14 22 23.65	-00 23 09.2	1695	SAB(rs)cd	12.63	0.075	3.4	04/18/01
NGC 5668	14 33 24.30	+04 27 02.0	1665	SA(s)d	12.2	0.071	3.3	04/23/01
NGC 5669	14 32 44.00	+09 53 31.0	1481	SAB(rs)cd	12.03	0.053	4.0	07/14/01
NGC 5774	14 53 42.60	+03 34 59.0	1648	SAB(rs)d	12.74	0.081	3.0	05/20/01
NGC 5789	14 56 35.52	+30 14 02.5	2002	Sdm	14.70	0.041	0.9	03/17/01
NGC 5964	15 37 36.30	+05 58 26.0	1552	SB(rs)d	12.6	0.113	4.2	05/02/01
ESO 138-10	16 59 02.96	-60 12 02.9	942	SA(s)cd	11.59	0.427	5.6	05/29/01
NGC 6509	17 59 25.36	+06 17 12.4	1926	Sd	13.10	0.375	1.6	07/03/00
NGC 6946	20 34 52.34	+60 09 14.2	310	SAB(rs)cd	9.61	0.663	11.5	12/03/00
ESO 187-51	21 07 33.09	-54 57 02.0	1158	SB(s)m	14.85	0.066	1.9	03/23/01
UGC 12082	22 34 11.54	+32 52 10.3	974	Sm	14.1	0.185	2.6	08/13/00
NGC 7418	22 56 36.00	-37 01 47.3	1287	SAB(rs)cd	12.30	0.031	3.5	06/01/01
NGC 7424	22 57 18.08	-41 04 19.0	765	SAB(rs)cd	10.96	0.021	9.5	06/01/01
ESO 290-39	23 03 29.14	-46 02 22.8	1337	SB(s)m	15.0	0.028	1.1	10/12/00
UGC 12732	23 40.39.80	+26 14 10.0	870	Sm:	13.8	0.172	3.0	05/14/01
ESO 241-6	23 56 13.08	-43 26 00.0	1219	SB(s)m	14.4	0.025	1.1	11/12/00
NGC 7689	23 33 16.11	-54 05 37.0	1744	SA(r)c	12.2	0.023	2.9	07/12/01
NGC 7741	23 43 53.65	+26 04 33.1	872	SB(s)cd	11.84	0.145	4.4	07/24/01
NGC 7793	23 57 49.75	-32 35 29.5	69	SA(s)d	9.98	0.038	9.3	04/19/01

Note. — Columns 1-3: object name and coordinates, as taken from the NASA Extragalactic Database (NED). Column 4: recession velocity, corrected according to the Virgo-centric infall model (Sandage & Tammann 1990), taken from the Lyon-Meudon Extragalactic Database (LEDA). Columns 5 and 6: galaxy morphological type and apparent total B-magnitude (NED). Column 7: Galactic foreground extinction (Schlegel et al. 1998), converted to I-band using the Cardelli et al. (1989) extinction law, and $R_V = 3.1$ (NED). Column 8: galaxy major axis diameter (NED). Column 9: date of observation.

Table 2. Nuclear Cluster Properties

(1) Galaxy	(2) Distance [Mpc]	(3) HWHM [$''$]	(4) HWHM [pc]	(5) R_u [$''$]	(6) m_I [mag]	(7) M_I [mag]	(8) μ_0 [mag]	(9) Type of fit
NGC 275	24.0	0.054	6.3	0.5	19.47±0.01	-12.54	15.312	u
NGC 300	2.2[1]	0.133	1.4	2.5	15.29±0.40	- 11.43	13.651	u
NGC 337a	14.3	0.058	4.0	0.6	20.94±0.01	-10.02	17.144	u*
NGC 428	16.1	0.046	3.6	0.9	17.95±0.01	-13.15	13.875	u
NGC 450	25.6	0.112	13.3	0.4	20.13±0.17	-11.90	16.584	u
ESO 80-6	17.5	-	-	-	-	-	-	fc
NGC 600	25.2	0.057	7.0	0.3	19.92±0.03	-12.16	15.712	u
NGC 853	20.2	0.054	5.3	0.25	19.90±0.04	-11.68	15.515	u
NGC 1042	18.2	0.052	4.6	0.2	18.40±0.29	-12.95	13.464	u
NGC 1313	4.4[2]	-	-	-	-	-	-	fc
ESO 358-5	20.1	0.055	5.4	1.0	20.10±0.06	-11.44	16.358	u*
ESO 418-8	14.1	0.052	3.6	0.3	20.54±0.01	-10.24	16.154	u
NGC 1493	11.4	0.058	3.2	0.5	17.17±0.03	-13.13	13.259	u
ESO 202-41	19.9	0.059	5.7	0.4	22.51±0.03	-9.01	18.277	u*
ESO 85-47	16.9	-	-	-	-	-	-	fc
ESO 204-22	14.4	-	-	-	-	-	-	fc
NGC 2139	23.6	0.066	7.5	0.25	19.28±0.29	-12.65	14.652	u
UGC 3574	23.4	0.065	7.4	0.5	20.04±0.18	-11.90	16.063	u
UGC 3826	27.8	0.074	10.0	0.2	21.60±0.02	-10.76	17.375	u
NGC 2552	9.9	0.053	2.6	1.0	18.04±0.01	-12.04	14.220	u
UGC 4499	12.5	0.072	4.4	0.3	21.97±0.63	-8.59	17.902	u*
NGC 2763	25.3	0.067	8.2	0.2	20.59±0.35	-11.56	15.350	u
NGC 2805	28.1	0.060	8.2	0.5	19.02±0.06	-13.32	14.987	u
UGC 4988	24.2	0.054	6.4	0.3	20.76±0.04	-11.20	16.397	u
UGC 5015	25.7	0.065	8.2	0.3	20.71±0.01	-11.37	16.686	u
UGC 5288	8.0	-	-	-	-	-	-	fc
NGC 3206	19.7	-	-	-	-	-	-	fc
NGC 3346	18.8	0.042	3.8	0.3	19.64±0.01	-11.78	15.106	u
NGC 3423	14.6	0.057	4.1	0.3	19.04±0.05	-11.84	14.876	u
NGC 3445	32.1	0.051	7.9	0.4	19.12±0.10	-13.42	14.794	u
NGC 3782	13.5	0.055	3.6	0.25	20.61±0.01	-10.07	16.134	u
NGC 3906	16.7	0.059	4.8	0.3	21.15±0.11	-10.01	16.759	u
NGC 3913	17.0	0.255	21.0	0.3	21.22±0.07	-9.96	17.256	u
A 1156+52	18.7	0.055	5.0	0.4	20.43±0.01	-10.98	16.19	u
ESO 504-30	23.9	0.056	6.5	0.3	20.70±0.05	-11.33	16.522	u
UGC 6931	20.7	0.052	5.2	0.5	21.91±0.12	-9.72	17.757	u′
NGC 4027	22.7	0.066	7.3	0.2	20.38±0.22	-11.48	15.335	u
NGC 4204	13.8	0.066	4.5	0.4	20.51±0.02	-10.26	16.590	u*
NGC 4299	16.8[3]	0.051	1.1	0.25	19.46±0.04	-11.73	14.912	u
NGC 4416	20.7	0.219	22.0	0.25	22.82±0.64	-8.81	17.415	u′
NGC 4411B	19.1	0.062	5.8	0.3	18.89±0.07	-12.57	14.892	u
NGC 4487	14.6	0.051	3.6	0.25	17.89±0.01	-12.97	13.391	u
NGC 4496A	25.3	0.048	6.0	0.3	20.08±0.02	-11.99	15.631	u′
NGC 4517A	22.2	-	-	-	-	-	-	fc
NGC 4540	19.8	0.069	6.6	0.3	19.25±0.02	-12.29	15.098	u
NGC 4618	10.7	0.098	5.1	0.5	18.74±0.06	-11.45	15.668	u
NGC 4625	11.7	0.097	5.5	0.3	19.76±0.08	-10.61	15.803	u

Table 2—Continued

(1) Galaxy	(2) Distance [Mpc]	(3) HWHM [″]	(4) HWHM [pc]	(5) R_u [″]	(6) m_I [mag]	(7) M_I [mag]	(8) μ_0 [mag]	(9) Type of fit
NGC 4701	11.0	0.044	2.4	0.5	16.81±0.07	-13.45	12.641	u
NGC 4775	22.4	0.056	6.1	0.3	18.04±0.05	-13.77	13.852	u
NGC 4904	17.2	-	-	-	-	-	-	fc
A 1301-03	19.7	-	-	-	-	-	-	ngf
IC 4182	7.4	-	-	-	-	-	-	ngf
ESO 444-2	22.1	-	-	-	-	-	-	fc
NGC 5068	8.7	0.106	4.5	1.0	17.55±0.05	-12.34	15.194	u
UGC 8516	16.5	0.089	7.2	0.4	20.18±0.09	-10.97	16.615	u
ESO 510-59	32.4	-	-	-	-	-	-	ngf
NGC 5477	8.1	-	-	-	-	-	-	fc
NGC 5585	8.2	0.063	2.5	0.5	18.24±0.03	-11.35	14.531	u
NGC 5584	24.2	0.075	8.8	0.2	22.53±0.58	-9.47	16.837	u
NGC 5789	28.6	-	-	-	-	-	-	fc
NGC 5668	23.8	0.054	6.3	0.4	18.86±0.06	-13.10	14.757	u
NGC 5669	21.2	0.123	12.6	0.25	21.66±0.01	-10.03	17.354	u*
NGC 5774	23.5	0.073	8.3	0.2	21.97±0.05	-9.97	17.369	u
NGC 5964	22.2	0.056	6.1	0.5	19.22±0.06	-12.62	15.210	u
ESO 138-10	13.5	0.085	5.6	0.5	16.68±0.13	-14.40	13.367	u
NGC 6509	27.5	0.043	5.8	0.25	19.49±0.07	-13.08	14.752	u
NGC 6946	5.5[3]	-	-	-	-	-		ngf
ESO 187-51	16.5	-	-	-	-	-	-	fc
UGC 12082	13.9	-	-	-	-	-	-	fc
ESO 290-39	19.1	0.070	6.5	0.3	22.52±0.01	-8.92	18.261	u′
NGC 7418	18.4	0.065	5.8	3.0	15.12±0.22	-16.23	13.027	u
NGC 7424	10.9	0.097	5.1	0.5	18.80±0.05	-11.41	15.650	u
UGC 12732	12.4	0.067	4.0	1.0	19.35±0.01	-11.29	15.888	u′
ESO 241-6	17.4	0.056	4.7	0.3	21.30±0.15	-9.93	16.884	u
NGC 7689	24.9	0.080	9.6	0.4	18.26±0.12	-13.75	14.576	u
NGC 7741	12.5	-	-	-	-	-	-	fc
NGC 7793	3.3[4]	0.096	1.5	4.0	14.00±0.03	-13.64	12.551	u

Note. — Columns 1: object name. Column 2: distance, derived from the recession velocity in Column 4 of Table 1 and assuming $H_o = 70\,\mathrm{km\,s^{-1}}$, if not noted otherwise. Columns 3 and 4: angular and physical observed half width at half maximum of the nuclear cluster (i.e. not corrected for PSF convolution). The conversion assumes the distances listed in Column 2. Column 5: aperture radius used to derive cluster luminosity. Column 6: apparent I-band magnitude of the nuclear cluster. Listed is the average value for the two background models as described in § 2.4, and half their difference as the uncertainty. Column 7: absolute I-band magnitude of the nuclear cluster, corrected for Galactic extinction as listed in Column 7 of Table 1. The distance modulus was derived from the distances in Column 2. Column 8: peak observed I-band surface brightness in a $0\farcs0455$ square pixel (i.e. not corrected for PSF convolution). Column 9: type of the isophotal fit: (u) - unconstrained, sometimes with increased isophote spacing (indicated by *), or over two separate radial ranges (indicated by $'$) (fc) - fixed ellipse center and ellipticity, (ngf) - no good fit.

References. — (1) Freedman et al. (1992), (2) de Vaucouleurs (1963), (3) Tully (1988), (4) Carignan (1985)

This figure "boeker_fig1_1.jpg" is available in "jpg" format from:

http://arXiv.org/ps/astro-ph/0112086v1

This figure "boeker_fig1_2.jpg" is available in "jpg" format from:

http://arXiv.org/ps/astro-ph/0112086v1

This figure "boeker_fig3_3.gif" is available in "gif" format from:

http://arXiv.org/ps/astro-ph/0112086v1

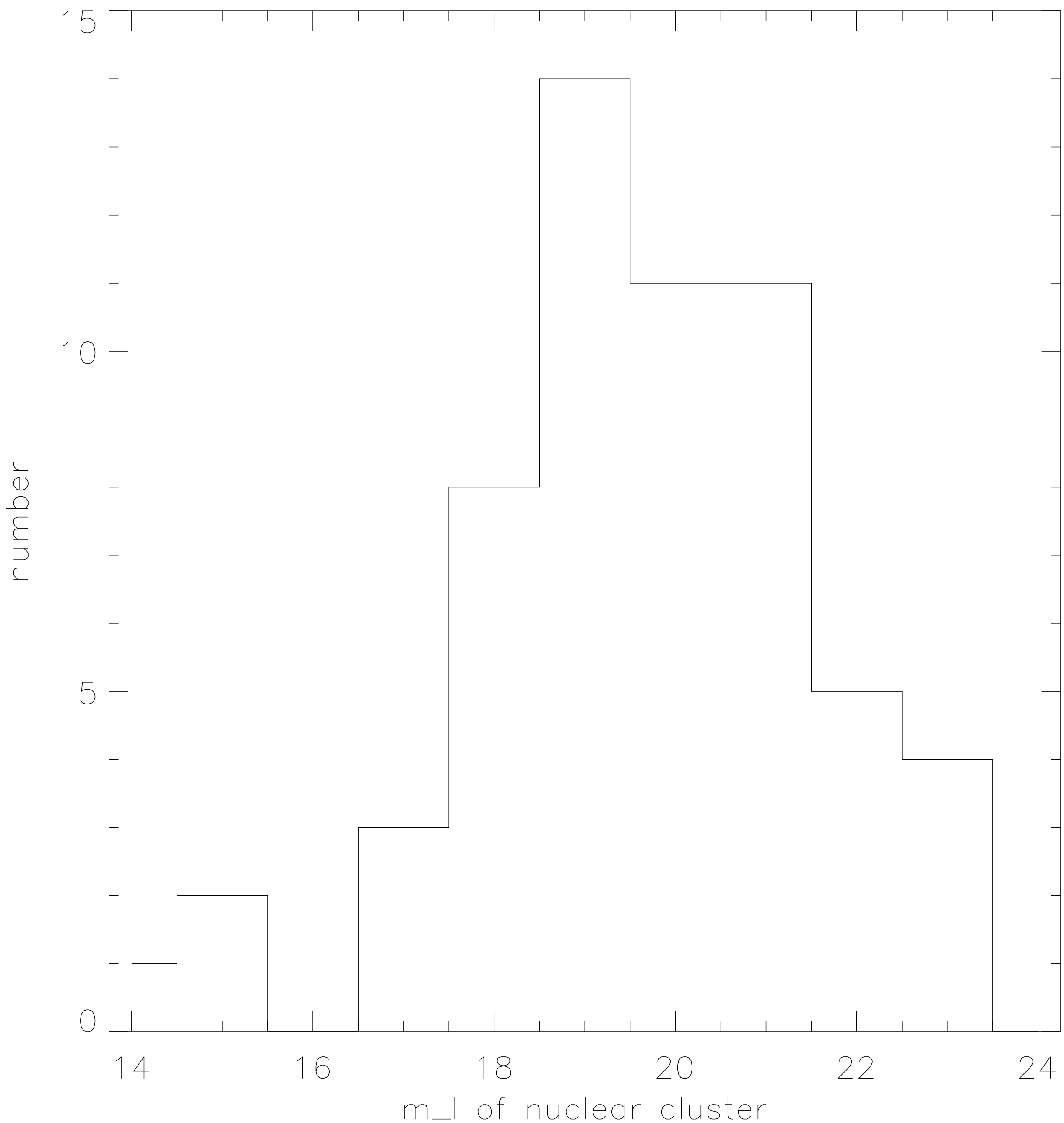

15
10
5
0
14
16
18
20
22
24
number
m_I of nuclear cluster

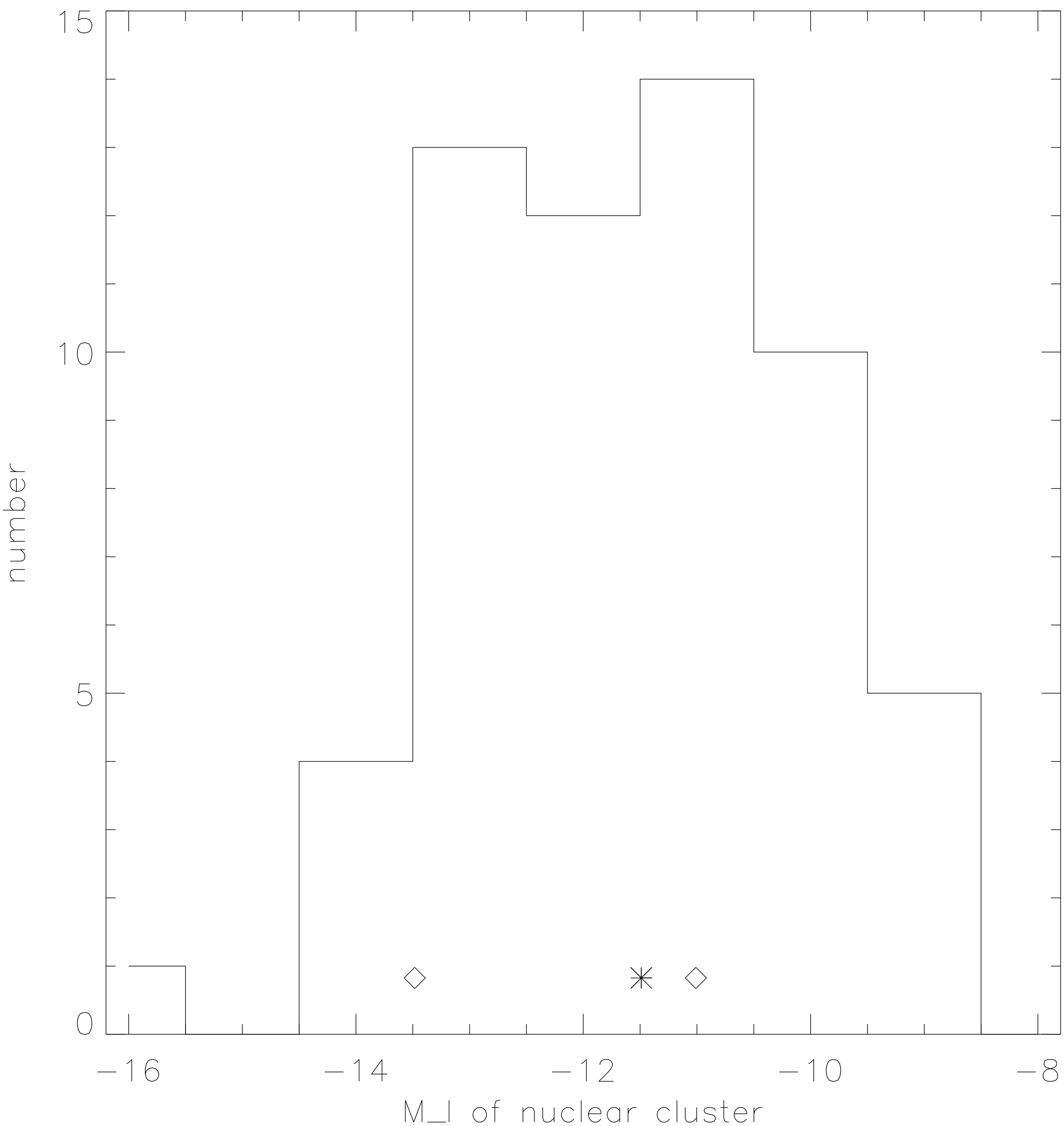

15
10
5
0
number
−16
−14
−12
−10
−8
M_I of nuclear cluster

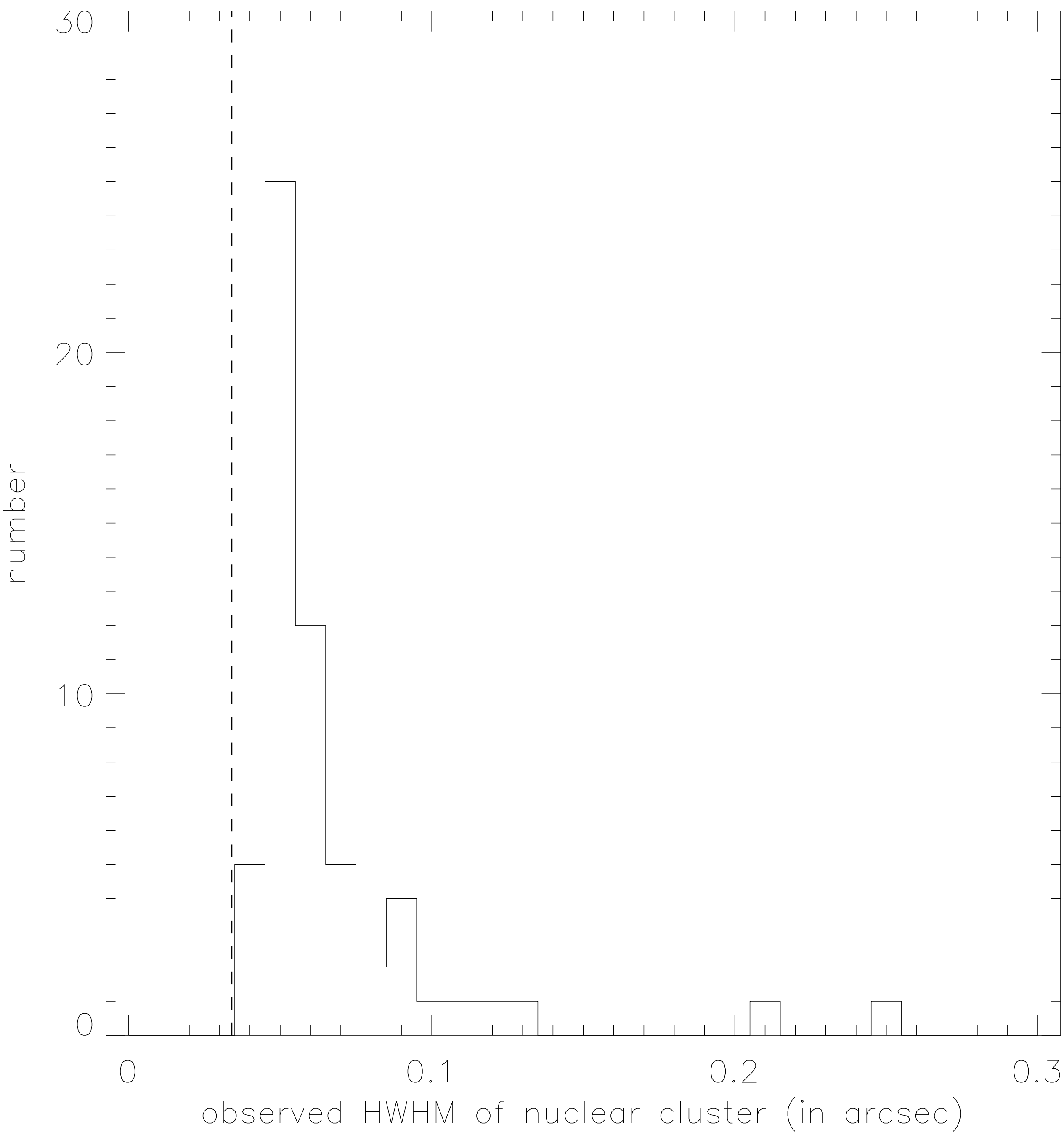

30
20
10
0
number
0
0.1
0.2
0.3
observed HWHM of nuclear cluster (in arcsec)

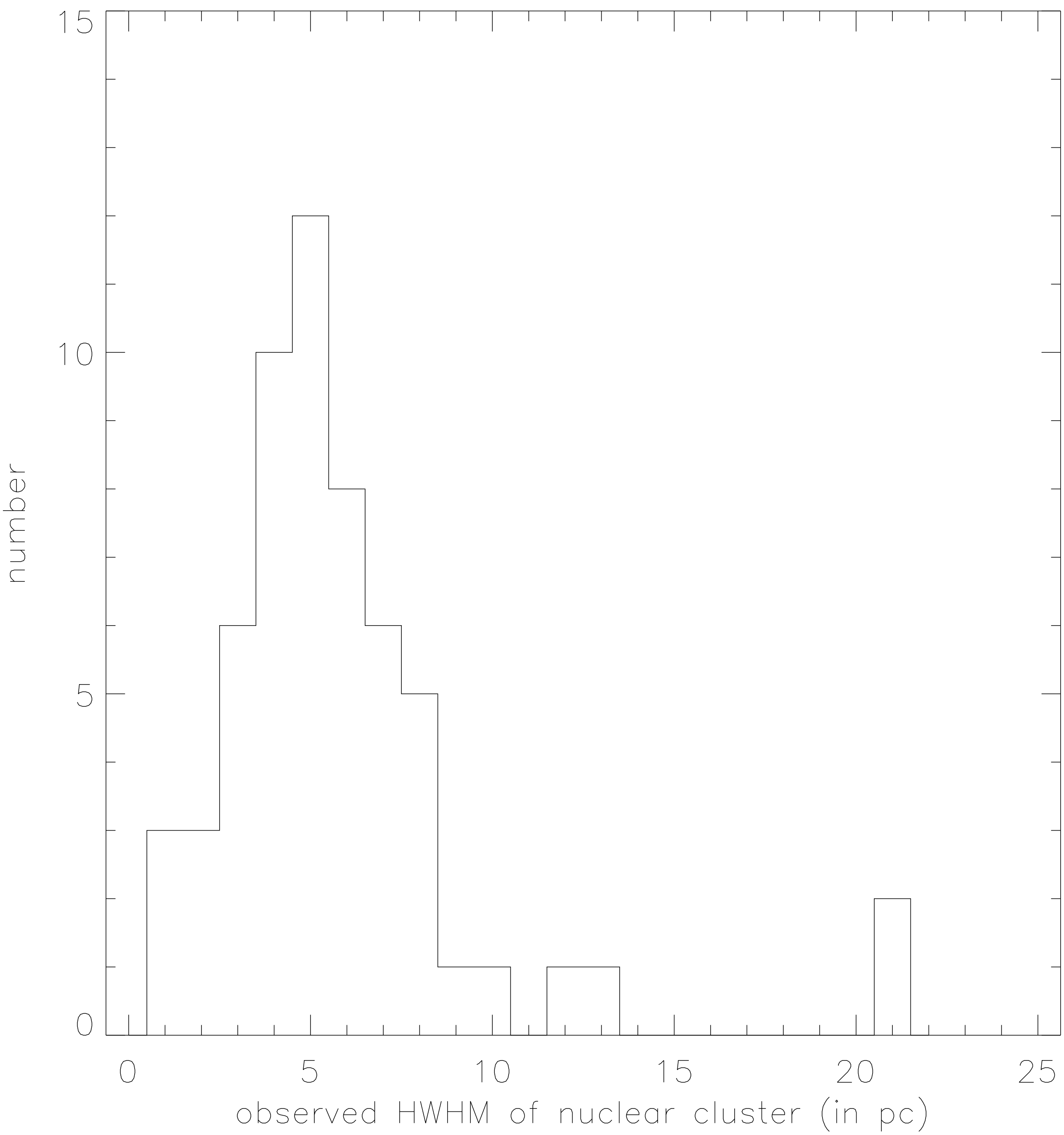

15
10
5
0
number
0
5
10
15
20
25
observed HWHM of nuclear cluster (in pc)

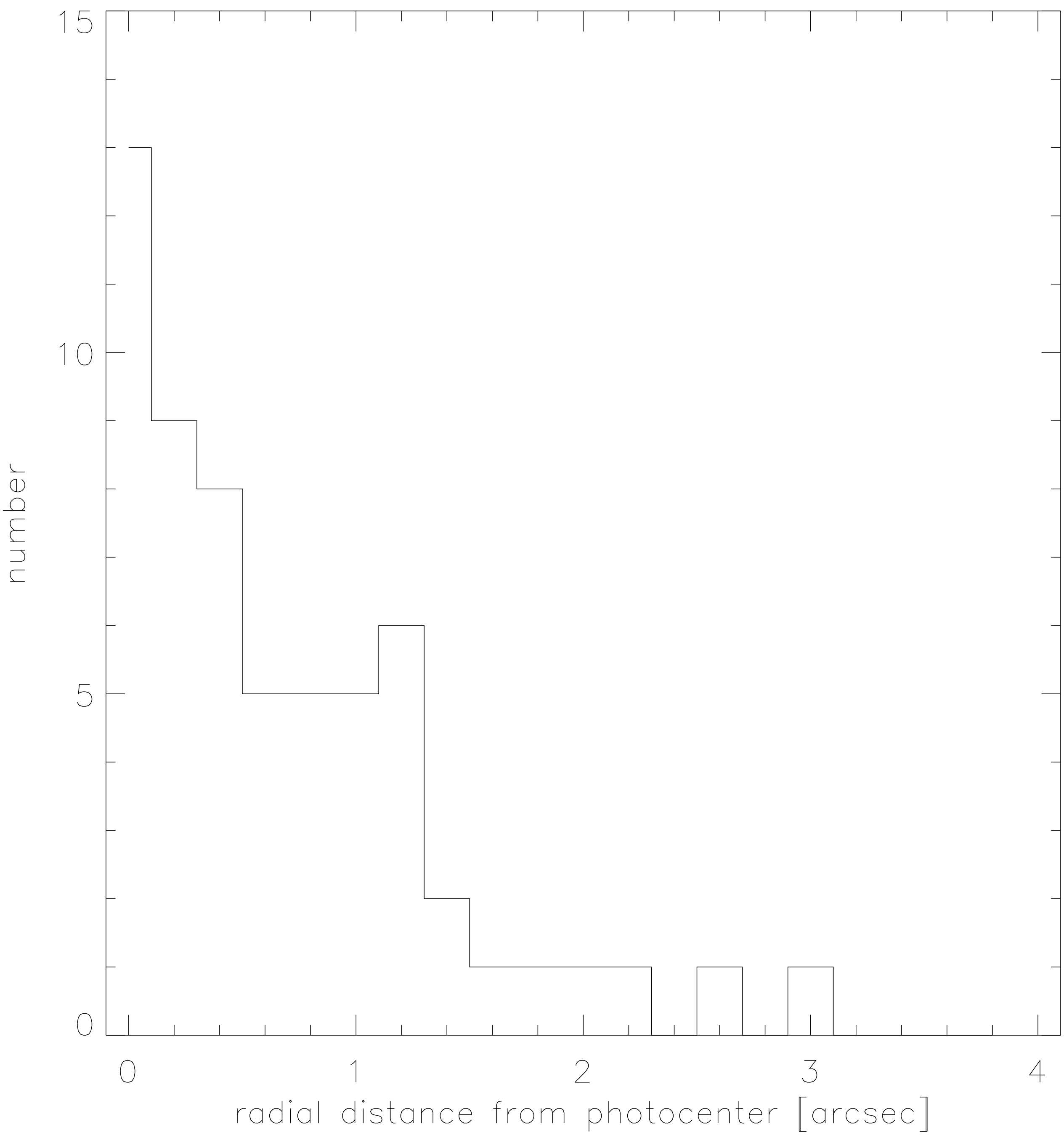

15
10
5
0
number
0
1
2
3
4
radial distance from photocenter [arcsec]

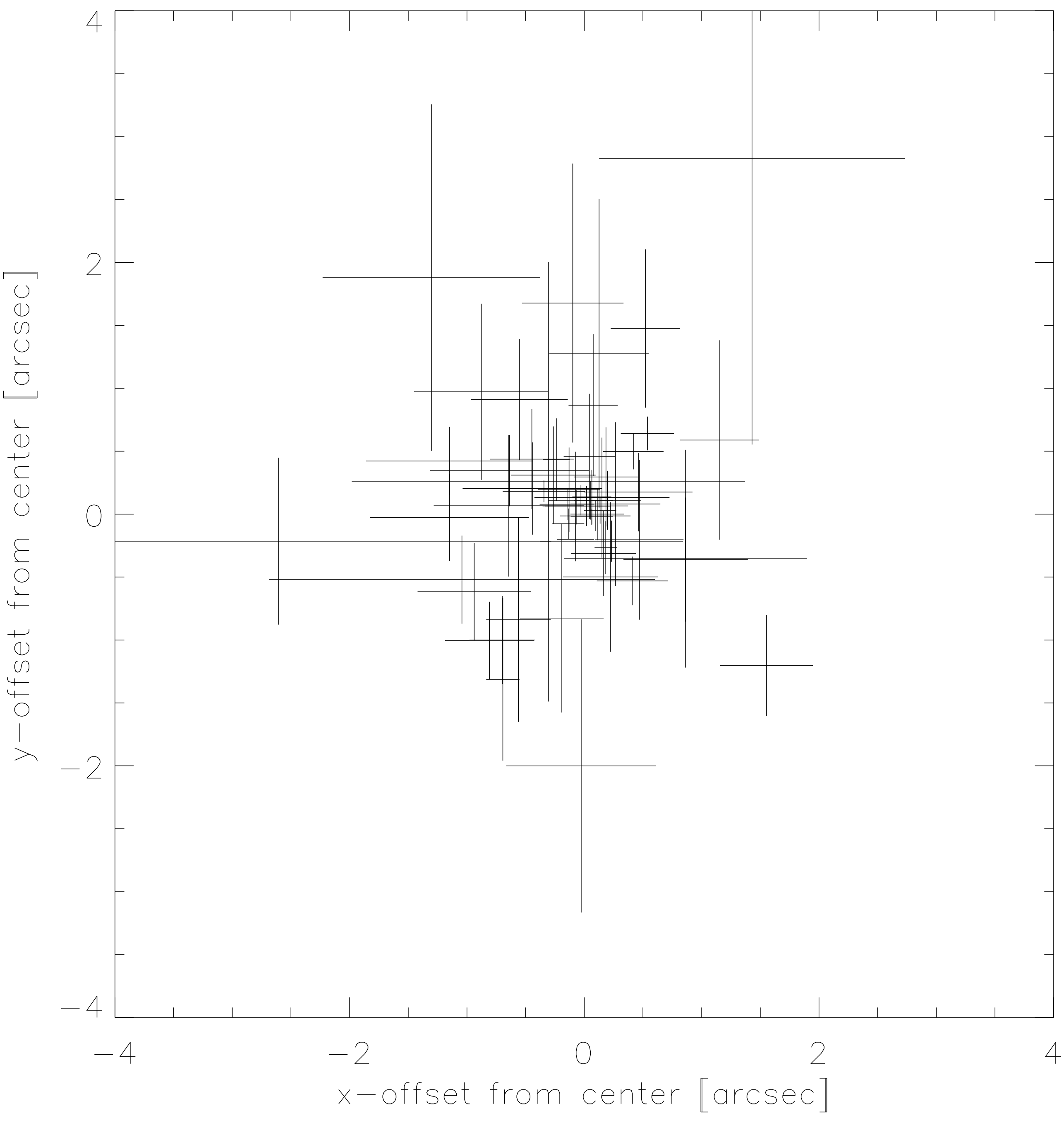

x−offset from center [arcsec]
y−offset from center [arcsec]

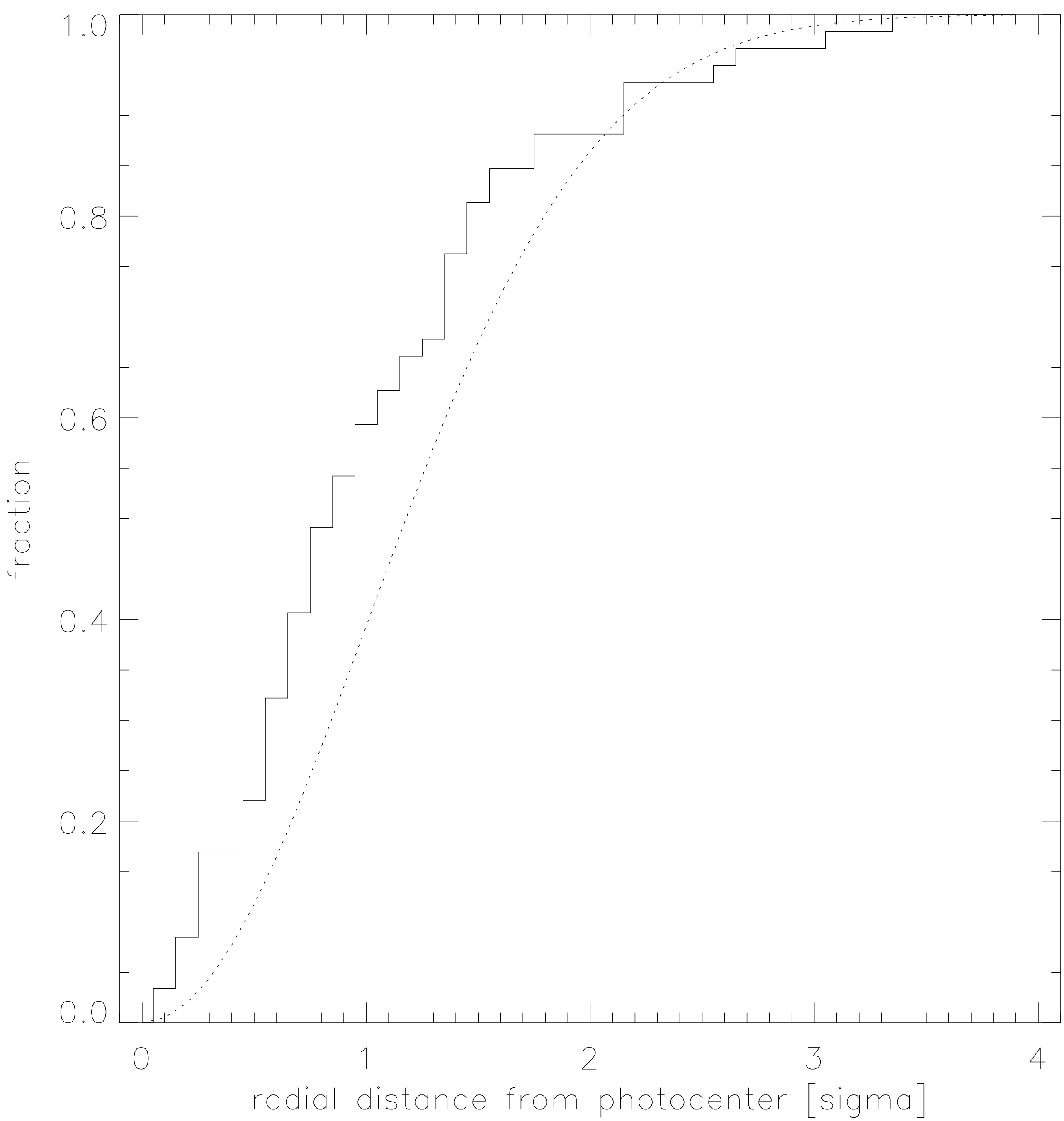

1.0
0.8
0.6
0.4
0.2
0.0
fraction
0
1
2
3
4
radial distance from photocenter [sigma]